Jahn-Teller effect in V4+ doped Gd3Ga5O12 garnet

M. Grinberg, A. Brenier, G. Boulon, C. Pedrini, C. Madej, A. Suchocki

Classification
Physics Abstracts
71.70C — 78.50 — 78.55

Jahn-Teller effect in V^{4+} doped $Gd_3Ga_5O_{12}$ garnet

M. Grinberg ([1]) A. Brenier ([2]), G. Boulon ([2]), C. Pedrini ([2]), C. Madej ([2]) and A. Suchocki ([3])

([1]) Institute of Physics, N. Copernicus University, Grudziadzka 5/7, 87-100 Torun, Poland
([2]) Laboratoire de Physico-Chimie des Matériaux Luminescents (*), Université Claude Bernard-Lyon I, 43 Bd 11 Novembre 1918, 69622 Villeurbanne Cedex, France
([3]) Institute of Physics, Polish Academy of Sciences, Al. Lotnikow 32/46, 02-668 Warszawa, Poland

Abstract. — We consider the static and dynamic E * ∈ and T * ∈ Jahn-Teller effects in order to analyze the absorption and emission spectra of octahedrally coordinated V^{4+} and absorption of tetrahedrally coordinated V^{4+}. Using two-dimensional configuration coordinate diagrams of octahedrally and tetrahedrally coordinated V^{4+} we are able to explain the structure of the emission and absorption spectra and the fluorescence kinetics measurements of V^{4+} doped GGG. Our calculations support the assumption that V^{4+} in tetrahedral sites is responsible for the additional absorption band in the red region.

1. Introduction.

It is well-known that the Ti^{3+} ion in various matrices, especially in sapphire, is suitable for tunable laser application in the near infrared range [1-3]. Another ion with the same electronic configuration, $3d^1$, is V^{4+}. Some studies were devoted to this ion in the past [4, 5] because of its possible applications as an active ion. More recently we have performed absorption, luminescence, luminescence excitation, decay kinetics and photoconductivity measurements of $Gd_3Ga_5O_{12}.V^{4+} \cdot Ca^{2+}$ (0.5 % mole) garnet [6]. We have shown that vanadium ions occupy both octahedral and tetrahedral sites. The main purpose of this paper is a theoretical analysis of these spectroscopic data. Details of crystal growth and experimental techniques are reported in our previous work [6].

In order to analyze the absorption and emission spectra of octahedrally coordinated V^{4+} and absorption of tetrahedrally coordinated V^{4+} we consider E * ∈ and T * ∈ electron-lattice couplings of the system in ^2E and $^2T_2$ state, respectively. Using the data obtained from the analysis of the dynamic E * ∈ Jahn-Teller effect we reproduce the two-dimensional

---

(*) Unité de recherche associée au CNRS n 442.

configuration coordinate diagrams of octahedrally and tetrahedrally coordinated V^{4+}, which allow us to explain the spectroscopic properties of vanadium doped GGG. We also consider the non-radiative internal conversion process which involves the ^2E and $^2T_2$ electronic manifolds in order to explain the results of fluorescence decay kinetics measurements. The presented theoretical analysis supports the assumption that the additional absorption band observed in the red region is due to the V^{4+} in tetrahedral sites.

2. Configuration coordinate model of V^{4+} ion in GGG lattice.

2.1 DERIVATION OF THE CONFIGURATIONAL COORDINATE DIAGRAMS. — The adiabatic configuration coordinate diagrams of the V^{4+} ion in the octahedral and tetrahedral sites are presented in this section. For both cases of octahedral and tetrahedral coordination, we have assumed that the dominant part of the electron-lattice interaction is the coupling of a d electron with a two-dimensional local lattice vibration mode of ϵ symmetry. In order to obtain the configuration coordinate diagrams, we have considered the contribution of the static Jahn-Teller distortion to the energy of $^2T_2$ and ^2E states described by the following Hamiltonians [7, 8] :

$$H_{J-T}(^2T_2) = L_T \begin{bmatrix} Q_\theta - \sqrt{3}\,Q_\epsilon & 0 & 0 \\ 0 & Q_\theta - \sqrt{3}\,Q_\epsilon & 0 \\ 0 & 0 & -2\,Q_\theta \end{bmatrix} \qquad (1)$$

and

$$H_{J-T}(^2E) = L_E \begin{bmatrix} -Q_\theta & Q_\epsilon \\ Q_\epsilon & Q_\theta \end{bmatrix} + K_E \begin{bmatrix} Q_\theta^2 - Q_\epsilon^2 & 2\,Q_\theta\,Q_\epsilon \\ 2\,Q_\theta\,Q_\epsilon & Q_\epsilon^2 - Q_\theta^2 \end{bmatrix}, \qquad (2)$$

respectively. Here we include the nonlinear electron-lattice coupling for the system in the ^2E state, whereas only the linear terms are taken into account for the $^2T_2$ state.

The absorption spectrum of octahedrally coordinated V^{4+} ions in GGG reveals a characteristic « camel back » structure, typical for large E $*$ ϵ Jahn-Teller effect. Therefore we start from an estimate of the Jahn-Teller stabilization energy for the system in the ^2E state, $E^0_{J-T}(E) = L_E^2/2$. We have calculated the vibronic structure of ^2E electronic manifold and the $^2T_2 \to {}^2E$ absorption spectrum, using the numerical procedure proposed by Longuet-Higgins, Opik, Pryce and Sack (LOPC) [9]. To obtain the convergent solutions for the energy region under consideration, we have numerically diagonalized the 120 × 120 (LOPC) matrix. In this part of the calculations we have assumed that the T $*$ ϵ Jahn-Teller effect and the nonlinear electron-lattice coupling of the system in the ^2E state are negligible. Using the phonon energy $\hbar\omega = 239\ \text{cm}^{-1}$ and the energy of the « zero-phonon » transition, $E^0 = 17\,800\ \text{cm}^{-1}$, we have reproduced the energies of the maxima of the absorption spectrum equal to the experimental ones with the Jahn-Teller stabilization energy $E^0_{J-T}(E) = L_E^2/2 = 3\,000\ \text{cm}^{-1}$ The calculated absorption spectrum is presented in figure 1 in comparison with the experimental absorption and excitation spectra of octahedrally coordinated V^{4+} The obtained value of the Jahn-Teller stabilization energy is slightly larger than in the case of octahedrally coordinated Ti^{3+} [10-14].

Since the static Jahn-Teller effect is large for the system in the ^2E state we can analyze the emission related to $^2E \to {}^2T_2$ transitions of the octahedral V^{4+} sites, by considering the Frank-Condon (vertical) transitions between the minimum of ^2E electronic manifold and the ground electronic manifolds. We relate the maxima of the emission, listed in table I (see also Fig. 2), to the particular transitions shown on the configuration coordinate diagram in figure 3a.
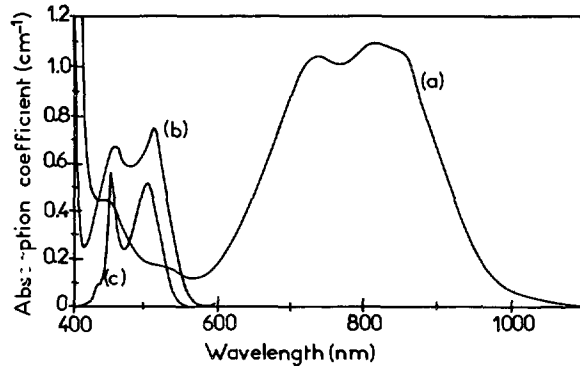
Fig. 1. — V^{4+} absorption and excitation spectra. Curves (a) and (b) correspond to absorption and excitation spectra, respectively, curve (c) corresponds to the calculated absorption spectrum.

Table I. — *Positions of the maxima in the absorption and emission of* GGG : V^{4+} *Asterisks correspond to the fitted data.*

Site	Emission (nm)		Absorption (nm)	
	experiment	theory	experiment	theory
octahedral	631.4 λ_3 698.1 λ_2 923.6 λ_1	641.0 698.1 * 923.6 *	447 λ_7 508 λ_8	447 * 508 *
tetrahedral			750 λ_4 818 λ_5 855 λ_6	658 673 879

It should be mentioned here that the nonlinear coupling with the lattice results in the stabilization of the distorted system in the ^2E state at the particular points in the configurational space [8, 12, 13]. Considering the new coordinate set : ρ and α, defined by :

$$\rho = [Q_\theta^2 + Q_\varepsilon^2]^{1/2} \quad \text{and} \quad \text{tg } \alpha = Q_\varepsilon/Q_\theta \qquad (3)$$

one obtains the potential energy minima placed at :

$$\rho = L_E/(1 - K_E) \quad \text{and} \quad \alpha = \pi/3, \pi \quad \text{and} \quad 5\pi/3 , \qquad (4)$$

whereas the saddle points are placed at :

$$\rho = L_E/(1 + K_E) \quad \text{and} \quad \alpha = 0, 2\pi/3 \quad \text{and} \quad 4\pi/3 , \qquad (5)$$

for K_E positive. When K_E is negative the minima and the saddle points replace each other. When the energies of the minima are much smaller than the energies of the saddle points, the lowest excited vibronic states may be approximated by two-dimensional harmonic oscillator states. Taking into account the minimum placed at $Q_\theta^0 = - L_E/(1 - K_E) Q_\varepsilon^0 = 0$
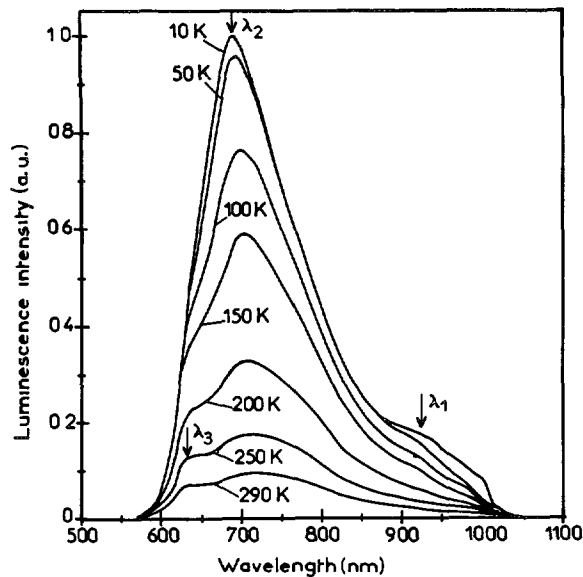
Fig. 2. — V^{4+} fluorescence spectra for different temperatures. λ_1, λ_2, and λ_3 correspond to the considered maxima of the emission bands (see Tab. I).
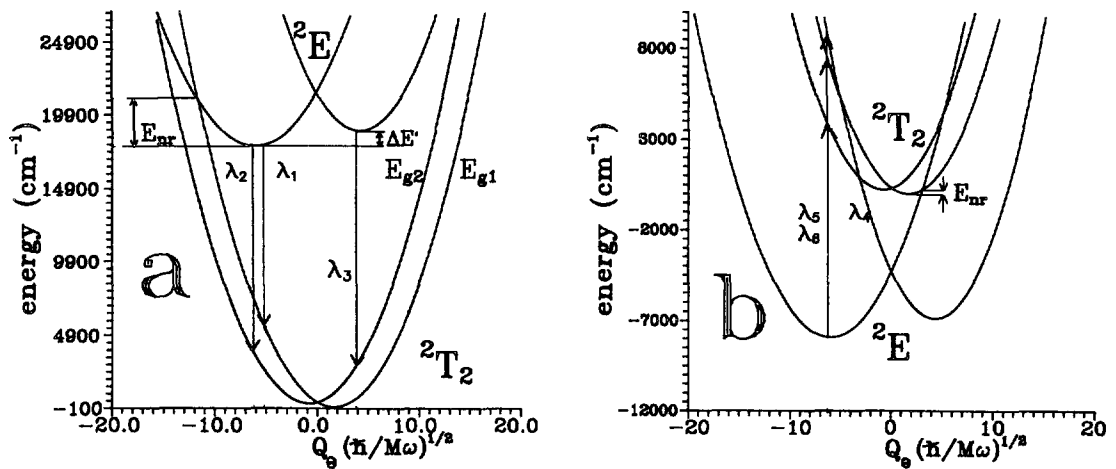

Fig. 3. — Configuration coordinate diagrams of V^{4+} a) octahedrally coordinated V^{4+}. b) tetrahedrally coordinated V^{4+} In both cases the diagrams present the sections for $Q_t = 0$. For details see text.

$(\rho = L_E/(1 - K_E)$, $\alpha = \pi$), one obtains the energies of respective modes [12] :

$$\hbar\omega_\theta = \hbar\omega_e \sqrt{(1 - K_E)} , \quad \hbar\omega_t = \hbar\omega_e \sqrt{(0.5 - 4.5 K_E^2 + 2 K_E)} . \tag{6}$$

Because the electron-lattice interaction for the system in $^2T_2$ state is given by diagonal matrix elements, $^2T_2$ electronic manifold splits into three parabolic surfaces corresponding to three components of the $^2T_2$ state with the energy minima placed at :

$$\rho = 2 L_T , \quad \alpha = 0 , \quad 2 \pi/3 \quad \text{and} \quad 4 \pi/3 . \tag{7}$$

Thus the vibronic structure of the ground state is given by the vibronic states of three two-dimensional harmonic oscillators. Since the electron-lattice coupling is linear in the ground state, the θ and ϵ modes are characterized by the same phonon energy.

A reproduced configuration coordinate diagram of octahedrally coordinated V^{4+} is presented in figure 3a. The energy difference between the minima and saddle points is indicated by $\Delta E'$.

The above remarks show that the fluorescence of the octahedral site is the sum of three independent, identical contributions related to the Frank-Condon transitions from the minimum energy of excited electronic manifold to the ground electronic manifolds. In our fitting procedure we have considered two emission bands with the maxima for $\lambda_1 = 923.6$ nm and $\lambda_2 = 688.1$ nm. These two bands are well separated in the low temperature fluorescence spectra (see Fig. 2). To focus our attention we considered the minimum of ^{2}E electronic manifold placed at $Q_\theta = -L_E/(1 - K_E)$, $Q_\epsilon = 0$, of the energy of the zero-phonon transition equal to $E^0 = 17\,800$ cm^{-1} Hence the values of parameters L_T and K_E have been obtained assuming that the maxima λ_1 and λ_2 correspond to the vertical transitions of the ground electronic manifolds to the vibronic states with the energies :

$$E_{g1} = 2\,L_T^2 + L_E^2/(1 - K_E) + 2\,L_T\,L_E/(1 - K_E) \qquad (8)$$

$$E_{g2} = 2\,L_T^2 + L_E^2/(1 - K_E) - L_T\,L_E/(1 - K_E)\,, \qquad (9)$$

respectively. It should be noted that the E_{g2} energy (as presented in the diagram) corresponds to a doubly degenerated state. Taking into account that $L_E = \sqrt{2\,E^0_{J-T}(E)}$, where $E^0_{J-T}(E)$ has been estimated from the absorption spectra, we have obtained the nonlinear coupling constant $K_E = 0.168$ and the Jahn-Teller stabilization energy of the ground ^{2}T$_2$ electronic manifold $E_{J-T}(^2T_2) = 2\,L_T^2 = 314$ cm^{-1} The important parameter which controls the deexcitation processes is the energy of crossover of the ground and excited electronic manifold, ΔE. For the octahedral site we have obtained $\Delta E_{oct} = 3\,100$ cm^{-1}

One can consider the temperature dependence of the emission spectrum. The population of the excited vibronic states of the of ^{2}E electronic manifold increases with temperature. Since the $\Delta E'$ is not too large (in our case $\Delta E' = 1\,040$ cm^{-1}) the states above the saddle points are also occupied at higher temperatures. One should notice that the vibronic wave functions of the energy states slightly above the saddle points strongly oscillate with α above the minima of the potential, whereas they are quite smooth above the saddle points. This yields that, for higher temperatures, the additional band related to the Frank-Condom transitions from the saddle points appears. The Frank-Condon transition from the saddle point to the doubly degenerated ground electronic manifold is indicated as λ_3 in the configurational coordinate diagram. In our case the corresponding wavelength is $\lambda_3 = 641$ nm. Actually, in the experiment an additional maximum is observed for $\lambda_3 = 631$ nm at higher temperatures. On the other hand the long wavelength maximum λ_1, and also, to some extent, the main maximum λ_2, disappear since the system is not well localized in the vicinity of the minima of the excited electronic manifold at higher temperatures. This effect is also observed in the experimental spectra.

To consider the tetrahedral V^{4+} site we have assumed that the crystal field parameter 10 Dq$_{tet}$, which is responsible for the splitting of the d level in the tetrahedral site, is related to the octahedral one, 10 Dq$_{oct}$, as follows :

$$10\,\mathrm{Dq}_{tet} = -\frac{4 * 10\,\mathrm{Dq}_{oct}}{9} \qquad (10)$$

The minus sign in the last equation is due to the reverse sequence of the ^{2}E and ^{2}T$_2$ states (in the tetrahedral coordination ^{2}E is the ground and ^{2}T$_2$ is the excited state). *The*

remaining parameters have been assumed to have the same values for the octahedral and tetrahedral sites. The configuration coordinate diagram for tetrahedrally coordinated V^{4+} ion is shown in figure 3b. Considering the absorption spectra one can see three maxima (λ_4, λ_5 and λ_6) related to the respective vertical Frank-Condon transitions indicated in the diagram. The calculated and the experimental values of the wavelengths are presented in table I. The agreement of the theoretical values with the experiment is only qualitative, however it should be mentioned that, changing the parameters of the diagram (10 Dq_{tet}, L_E, K_E, L_T) by only a few percent we were thus able to fit the red part absorption spectrum very accurately. There is additional proof which supports the model. One can see that the large E $*$ ϵ Jahn-Teller effect in the tetrahedral site results in very effective quenching of luminescence. It is due to the very low energy of the ground and excited electronic manifolds crossover. ΔE_{tet} is equal to 200 cm^{-1} approximately, in our case (it is smaller than the phonon energy). Thus, in the tetrahedral sites, the non-radiative internal conversion processes are much more probable than the radiative deexcitation. It is a reason for lack of fluorescence related to tetrahedrally coordinated V^{4+} in GGG.

2.2 NONRADIATIVE TRANSITIONS TEMPERATURE DEPENDENCE OF RADIATIVE DECAY TIME OF GGG : V^{4+} — Temporal evolution of the octahedral V^{4+} fluorescence is not exponential at all temperatures in the range of 10-300 K (see Fig. 4). Because of the large spectral overlap between this fluorescence and the tetrahedral V^{4+} sites absorption an efficient energy transfer from the octahedral V^{4+} ions can occur. We have been able to reproduce the experimental decays of fluorescence for different temperatures using Inokuti-Hirayama's [15] expression :

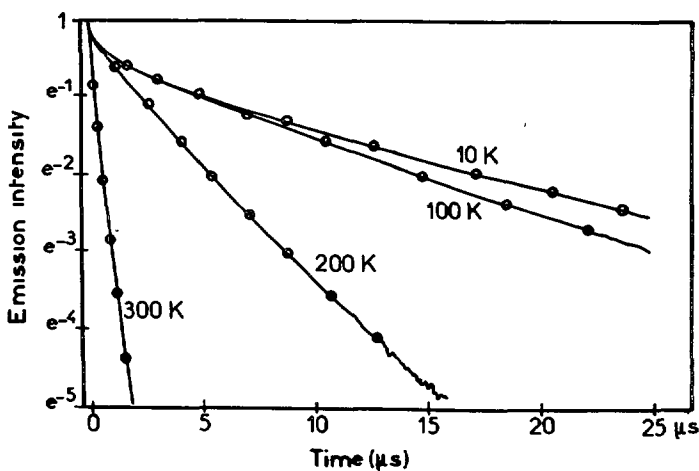$$I(t) = I_0 \, e^{-t/\tau - b(t/\tau)^{1/2}} \tag{11}$$

Fig. 4. — Experimental V^{4+} fluorescence decays for different temperatures. The circles correspond to the fit to Inokuti-Hirayama model.

Here τ is the decay time of the octahedral V^{4+} ion fluorescence and b is a parameter related to the tetrahedral V^{4+} ion concentration and to the strength of the interaction between donors and acceptors. The value of τ has been found to be temperature dependent, whereas b has been found to be a constant temperature independent. We have found $b = 0.81$. The computed values of τ are represented by circles in figure 5. A very rapid decrease of the
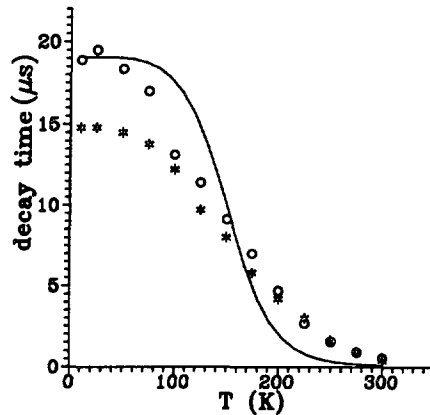
Fig. 5. — V^{4+} fluorescence decay time *versus* temperature. Asterisks correspond to the data obtained from fitting the decay after a long time. Circles correspond to data obtained from the Inokuti-Hirayama theory. The solid curve corresponds to the decay time calculated from the formula (20) (see text).

V^{4+} fluorescence decay time for temperatures above 100 K occurs. This effect can be explained using the configuration coordinate diagram of octahedrally coordinate V^{4+} ion presented in figure 3a. One can see that the lower component of ^{2}E crosses the upper component of the ground ^{2}T$_2$ state at the energy $E_{nr} = 3\ 100$ cm^{-1} This energy barrier is rather small (for the sake of comparison the respective value for octahedrally coordinated Ti^{3+} in sapphire has been estimated to be equal to 7 700 cm^{-1} [11] or 4 500 [12]). To consider the internal conversion non-radiative processes more exactly we have used the model which has been proposed for describing the non-radiative processes in the Ti^{3+} [13]. The non-radiative transition probability is calculated as the probability of the internal conversion process which takes place between the vibronic states of the excited and ground electronic manifolds with the same energy. For particular pair of the vibronic states this probability is given by :

$$T_{eg}^{NM} = 2\ \pi/\hbar\,(\hbar\omega)^{-1}\big|\,\langle\!\langle\,\Phi_e^N|H'|\Phi_g^M\rangle\!\rangle\,\big|^2\,\delta\,(E_e^N - E_g^M)\,, \tag{12}$$

where $\Phi_e^N(q,\,Q)\ \Phi_g^M(q,\,Q)$, are the Born-Oppenheimer wave functions defined as follows :

$$\Phi_{eg}^{NM}(q,\,Q) = \varphi_{eg}(q)\,\chi_{eg}^{NM}(Q)\,, \tag{13}$$

where φ and χ correspond to the electronic and vibronic parts of the functions, respectively. $N,\,M$ correspond to the vibronic quantum numbers, and $q,\,Q$ are the electronic and ionic (configuration) coordinate sets, respectively. $\langle\!\langle\ \rangle\!\rangle$ denotes the integration over q and Q space, δ is the Dirac delta function, $\hbar\omega$ is the phonon energy. Since H' is the perturbation Hamiltonian which mixes only the electronic parts of the wave functions, one can simplify relation (12) :

$$T_{eg}^{NM} = \tau_0^{-1}\big|F_{eg}^{NM}\big|^2\,\delta\,(E_e^N - E_g^M)\,, \tag{14}$$

where the parameter τ_0^{-1}, usually called the frequency factor, is given by :

$$\tau_0^{-1} = 2\ \pi/\hbar\,(\hbar\omega)^{-1}\big|\,\langle\varphi_e|H'|\varphi_g\rangle\,\big|^2 \tag{15}$$

F_{eg}^{NM} is the vibronic overlap integral related to the N and M vibronic states.

In the case of Ti^{3+} doped sapphire the perturbation Hamiltonian, H', has been found to be the Hamiltonian of the spin-orbit interaction which mixes the electronic parts of the wave functions of ^2E and $^2T_2$ states. We have assumed the same origin of perturbation that in the case of V^{4+}. Actually, the matrix elements of the spin-orbit Hamiltonian for V^{4+} are slightly greater than those for Ti^{3+} since vanadium is a smaller ion. We have used $|\langle \varphi_e | H' | \varphi_g \rangle| = 95 \text{ cm}^{-1}$ (80 cm^{-1} for Ti^{3+}, see Ref. [13]). Then, using equation (15) we have obtained $\tau_0^{-1} = 4 \times 10^{13} \text{ s}^{-1}$

To obtain the vibronic overlap integrals we have approximated the vibronic states related to the ground and excited electronic manifolds by harmonic oscillator wave functions corresponding to θ and ε modes :

$$\chi_{eg}^{NM}(Q) = \sum_{k=0}^{NM} \beta_{eg}^{N-k\,M-k}(Q_\theta)\, \beta_{eg}^{k}(Q_\varepsilon). \tag{16}$$

Hence :

$$F_{eg}^{NM} = \sum_{k}^{N} \sum_{k'}^{M} \langle \beta_e^{N-k} | \beta_g^{M-k'} \rangle_\theta \langle \beta_e^{k} | \beta_g^{k'} \rangle_\varepsilon \tag{17}$$

Here $\langle\ \rangle$ denotes the integration over respective configuration coordinates, θ or ε. Since the functions β are the one-dimensional harmonic oscillator wave functions, one calculates the overlap integrals in equation (17) using the Manneback recurrence approach [16]. One should discuss the validity of the above simplification for the case of the vibronic states related to the excited, ^2E electronic manifold. It has been shown [17] that the vibronic wave functions of highly excited states are very well approximated by harmonic oscillator wave functions, near the energy surface. Thus one-dimensional harmonic oscillator wave functions $\beta(Q_\theta)$ can describe quite accurately the vibrations of the system in θ direction. In ε direction the system can be described by one-dimensional harmonic oscillator wave functions $\beta^n(\varepsilon)$ when n corresponds to an energy smaller than the energy of the saddle points. On the other hand, since the energy of the crossing point in configurational coordinate diagram in figure 3a corresponds in fact to the lowest energy of the ground and excited manifold crossing we are mostly interested in the values of the overlap integrals of the $\beta(\theta)$ functions. The overlap integrals of $\beta(\varepsilon)$ yield significant contributions only for a few lowest vibronic quantum numbers. Therefore the approximation which yields relation (17) seems to be well grounded.

The total nonradiative decay, τ_{nr}, can be calculated considering the system thermalized in the excited electronic state. One obtains :

$$\tau_{nr}^{-1}(T) = \tau_0^{-1} \sum_N S^N(T) \left| F_{eg}^{NM} \right|^2 \delta(E_e^N - E_g^M), \tag{18}$$

where $S^N(T)$ is the Boltzmann occupation number, for a two-dimensional vibronic system defined by :

$$S^N(T) = \exp(-N\hbar\omega_e/kT)\left[\sum_{N'} (N'+1)\exp(-N'\hbar\omega/kT)\right]^{-1}$$

$$= \exp(-N\hbar\omega_e/kT)\,[1 - \exp(-\hbar\omega_e/kT)]^{-2} \tag{19}$$

$\hbar\omega_e$ is the average energy of phonons related to the excited electronic manifold.

One can compare our approach with the Struck and Fonger (S&F) model [18, 19]. In fact equation (18) is equivalent to the result of Struck and Fonger. The difference is in the dimension of considered vibronic systems (Struck and Fonger have considered one-dimension-

al oscillators). Thus, when we restrict the system to one dimension we obtain exactly the Struck and Fonger results.

To analyze the fluorescence kinetics we have assumed that the total fluorescence decay time, τ, is related to the radiative, τ_{rad}, and nonradiative, τ_{nr}, decays as follows :

$$\tau^{-1} = \tau_{rad}^{-1} + \tau_{nr}^{-1} \tag{20}$$

Here τ_{nr} has been calculated using equation (18) and the radiative decay time has been assumed to be $\tau_{rad} = 20 \ \mu s$. The result of our calculations is presented in figure 5. Here the « experimental decay times » are presented as circles and asterisks. The values corresponding to the circles have been obtained from the nonexponential fluorescence decays using Inokuti-Hirayama model, whereas data indicated by asterisks have been obtained from the experimental decays by fitting to its long time parts.

The large probability of a non-radiative internal conversion process in highly excited vibronic states of the excited ^2E electronic manifold yields the significant difference between the absorption and excitation spectra of octahedrally coordinated V^{4+} In both cases (excitation and absorption) we observe two bands with the maxima cooresponding to the $\lambda_7 = 447$ nm ($\hbar\Omega_7 = 22\ 370$ cm^{-1}) and $\lambda_8 = 508$ nm ($\hbar\Omega_8 = 19\ 685$ cm^{-1}).

In the absorption spectrum the band with the maximum $\hbar\Omega_7$ is stronger than the second one, whereas in the excitation spectrum the band with the maximum $\hbar\Omega_8$ is evidently much stronger. This effect can be explained by a rapidly increasing probability of a non-radiative internal conversion process with an increasing energy of the vibronic states of the ^2E electronic manifold. Actually the energies $\hbar\Omega_7$ and $\hbar\Omega_8$ correspond to the excitation above and below the crossing point of the ground and excited electronic manifolds, respectively. One considers the kinetics of the deexcitation processes using the configuration coordinate diagram, presented in figure 6a. We distinguish the fast processes which take place before thermalization of the system in the ^2E state and the slow processes which take place after the system reaches thermal equilibrium. The fast processes are : the internal conversion of the system from highly excited vibronic state of ^2E electronic manifold into the ground electronic manifold, described by the transition probability $P_{inter} = T_{eg}^{NM}$ (Eq. (14)), and the inter-
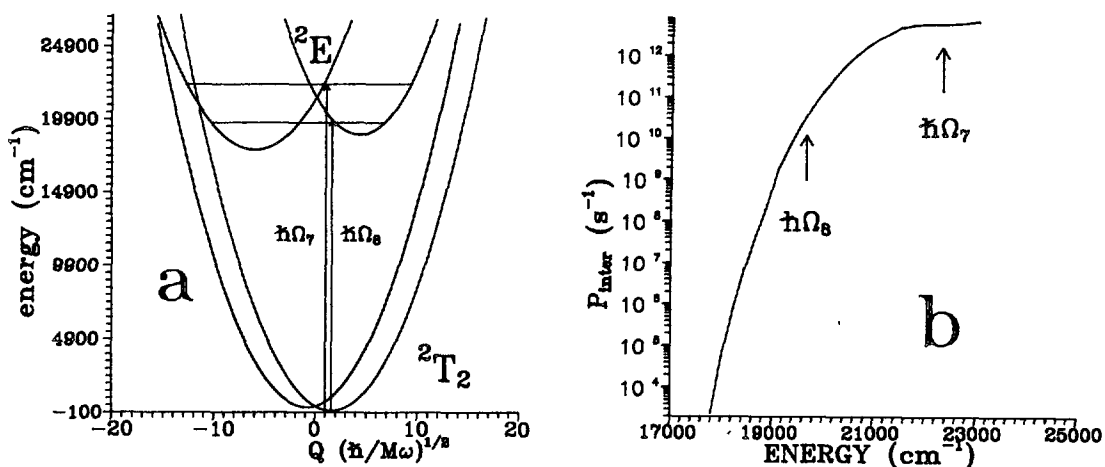

Fig. 6. — a) Configuration coordinate diagram of octahedrally coordinated V^{4+}. b) Absolute value of the internal conversion non-radiative transition probability *versus* absolute energy of the initial vibronic state. The energy of the minimum of the ground electronic manifold is taken to be zero.

configurational nonradiative transitions « inside » ^2E electronic manifolds, described by the transition probability P_{intra}. After thermalization in the ^2E state the system can relax due to the emission of photons, with probability $P_{\text{rad}}^{\text{ter}} = \tau_{\text{rad}}^{-1}$, or due to the nonradiative transitions with probability given by $P_{\text{nr}}^{\text{ter}} = \tau_{\text{nr}}^{-1}$ (see Eq. (18)). In detail the kinetics of these processes, in the steady state, is given by the following relations :

$$I_{\text{ex}}(\hbar\Omega)\,\mu(\hbar\Omega) = N_1(\hbar\Omega)[P_{\text{inter}}(\hbar\Omega) + P_{\text{intra}}] \tag{21}$$

$$N_1(\hbar\Omega)\,P_{\text{intra}}(\hbar\Omega) = N_2(\hbar\Omega)\,[P_{\text{rad}}^{\text{ter}} + P_{\text{nr}}^{\text{ter}}]\,. \tag{22}$$

Here μ is the fraction of absorbed photons, I_{ex} is the intensity of incident light and N_1 and N_2 are numbers of non-thermalized and thermalized V^{4+} ions, respectively. The intensity of the normalized excitation spectra is given by :

$$I_{\text{e}}(\hbar\Omega) = N_2(\hbar\Omega)\,P_{\text{rad}}^{\text{ter}}/I_{\text{ex}}(\hbar\Omega)\,. \tag{23}$$

In forms (21-23) we have indicated directly which quantities are dependent on the energy of absorbed photons.

Since $N_2(\hbar\Omega)$ can be obtained from (21) and (22) one can easily calculate the quantum yield of octahedrally coordinated V^{4+} ion, $\gamma(\hbar\Omega)$:

$$\gamma(\hbar\Omega) = I_{\text{e}}(\hbar\Omega)/\mu(\hbar\Omega) = \frac{P_{\text{rad}}^{\text{ter}}}{P_{\text{rad}}^{\text{ter}} + P_{\text{nr}}^{\text{ter}}}\;\frac{P_{\text{intra}}}{P_{\text{inter}}(\hbar\Omega) + P_{\text{intra}}} \tag{24}$$

Using (14) we have calculated the absolute value of $P_{\text{inter}}(\hbar\Omega)$. The results of this calculation are shown in figure 6b. One can see that the value of $P_{\text{inter}}(\hbar\Omega)$ increases about three orders of magnitude in the energy region between $\hbar\Omega_8$ and $\hbar\Omega_7$, and for the photon energy equal $\hbar\Omega_7$ can be comparable to the probability of an intra-configurational non-radiative transition. Actually equation (24) can be used for estimating of the absolute value of the probability of the non-radiative intra-configurational deexcitation, P_{intra}. One can assume that for the excitation energy $\hbar\Omega_8$ $P_{\text{inter}}(\hbar\Omega_8)$ is much smaller then P_{intra}. Thus approximating $\gamma(\hbar\Omega_8)$ by $\dfrac{P_{\text{rad}}^{\text{ter}}}{P_{\text{rad}}^{\text{ter}} + P_{\text{nr}}^{\text{ter}}}$ one obtains :

$$R = \gamma(\hbar\Omega_7)/\gamma(\hbar\Omega_8) \cong \frac{P_{\text{intra}}}{P_{\text{inter}}(\hbar\Omega_7) + P_{\text{intra}}} \tag{25}$$

The analysis of the absorption and excitation spectra yields $R \cong 0.5$, thus

$$P_{\text{inter}} \cong P_{\text{intra}}(\hbar\Omega_7) \cong 7 \times 10^{12}\ \text{s}^{-1}$$

3. Conclusions.

Since the energetic structure of V^{4+} ion in GGG is given by the properties of d^1 electron in the crystal field, one supposes that the spectroscopic properties of such a system are very similar to those one obtains using Ti^{3+} (also $3d^1$ system) as a dopant. Actually, we have found a close relation between the octahedrally coordinated V^{4+} and Ti^{3+} Especially, in both cases, the large E $*$ $\in$ Jahn-Teller effect results in the specific lineshapes of the absorption, excitation and fluorescence spectra. However, the structure in the emission spectra in the case of vanadium doped GGG (the spectrum consists of several broad bands whose relative intensities

depend on temperature) needs additional consideration of the splitting of the ground $^2T_2$ state. Although the Jahn-Teller splitting of $^2T_2$ state has been reported also for Ti^{3+} [11-13], we need a more efficient $T * \epsilon$ Jahn-Teller effect to explain all the details in the spectra of V^{4+} Our calculations show that, in the case of V^{4+}, the electron-lattice coupling is stronger then in the case of Ti^{3+}. This is true also in the case of the ^2E state, where the Jahn-Teller stabilization energy obtained for V^{4+} is greater than that predicted for Ti^{3+} [12-14]. This is the main reason why, in octahedrally coordinated V^{4+}, the non-radiative internal conversion process is much more important. It fact, in V^{4+}, the radiationless deexcitation dominates above 100 K, whereas for Ti^{3+} the critical temperature is about 300 K [10-14].

However, the main difference between the garnets doped with Ti^{3+} and the ones doped with V^{4+} is the large fraction of V^{4+} ions in the tetrahedral sites (see [20] for $Y_3Al_5O_{12} \cdot V^{4+}$). This might be due to the smaller ionic radius of $V^{4+} \cdot 0.59$ Å whereas 0.67 Å for Ti^{3+} Using the results of crystal field theory we have shown that the absorption band of tetrahedrally coordinated V^{4+} overlaps with the emission related to the octahedral sites. On the other hand the large electron-lattice coupling yields no emission related to the V^{4+} in tetrahedral sites. Thus the tetrahedrally coordinated vanadium is a typical fluorescence quenching center.

Acknowledgments.

References

[1] Moncorge R., Boulon G., Vivien D., Lejus A. M., Collongues R., Djevahirdjian V. and K., Cagnard R., *IEEE J. Quantum Electron.* **24b** (1988) 1049.

[2] Sanchez A., Strauss A., Aggarwal R., Fayet R., *IEEE J. Quantum Electron.* **24** (1980) 995.

[3] Schulz P. A., Henion S. R., *IEEE J. Quantum Electron.* **27** (1991) 1039.

[4] Weber M. J., Riseberg L. A., *J. Chem. Phys.* **55** (1971) 2032.

[5] Champagnon B., Duval E., *J. Phys C : Sol. State Phys.* **12** (1979) L425.

[6] Suchocki A., Brenier A., Pedrini C., Boulon G., *J. Phys. IV France,* supplément au *J. Phys. III France* **1** (1991) C7-323.

[7] Englman R., The Jahn-Teller Effect in Molecules and Crystals (Wiley-Interscience, London, New York, Sydney, Toronto, 1972).

[8] Bill H., The Dynamical Jahn-Teller Effect in Localized Systems, Yu. E. Perlin, M. Wagner Eds. (North Holland New York, 1984) p. 702.

[9] Longuet-Higgins H. C., Opik U., Pryce M. H. L., Sack R. A., *Proc. R. Soc. London, Ser. A* **244** (1958) 1.

[10] Gahter B. F., Koningstein J. A., *J. Chem. Phys.* **60** (1974) 2003.

[11]' Albers P., Stark E., Huber G., *J. Opt. Soc. AM.* **B 3** (1986) 134.

[12] Grinberg M., Mandelis A., Fieldsted K., Othonos A., *Phys. Rev. B* in press.

[13] Grinberg M., Mandelis A., Fieldsted K., *Phys. Rev. B* in press.

[14] Bantien F., Albers P., Huber G., *J. Lumin.* **36** (1987) 363.

[15] Inokuti M., Hirayama F., *J. Chem. Phys.* **43** (1965) 1978.

[16] Manneback C., *Physica* **XVII** (1951) 1001.

[17] The approximate wave functions of a highly vibronic states for dynamic Jahn-Teller systems have been calculated M. C. ; O'Brien M., *J. Phys. Colloq. France* **37** (1976) C9-2375.

[18] Struck C. W., Fonger W. H., *J. Lumin.* **10** (1975) 1.

[19] Fonger W. H., Struck C. W., *Phys. Rev.* **B 11** (1975) 2351.

[20] Manuilov N., Peshev P., *Mat. Res. Bull.* **24** (1989) 1549.